






Chemical characteristics of the products of the complexation reaction between copper(II) and a tetra-aza macrocycle in the presence of chloride ions

Kimberly M. Lincoln, Netzahualcóyotl Arroyo - Currás, Hannah M. Johnston, Travis D. Hayden, Brad S. Pierce, Nattamai Bhuvanesh & Kayla N. Green


To cite this article: Kimberly M. Lincoln, Netzahualcóyotl Arroyo - Currás, Hannah M. Johnston, Travis D. Hayden, Brad S. Pierce, Nattamai Bhuvanesh & Kayla N. Green (2015) Chemical characteristics of the products of the complexation reaction between copper(II) and a tetra-aza macrocycle in the presence of chloride ions, *Journal of Coordination Chemistry*, 68:16, 2810-2826, DOI: [10.1080/00958972.2015.1068935](https://doi.org/10.1080/00958972.2015.1068935)


To link to this article: <http://dx.doi.org/10.1080/00958972.2015.1068935>

 View supplementary material 

 Accepted author version posted online: 06 Jul 2015.
Published online: 30 Jul 2015.


 Submit your article to this journal 

 Article views: 68

 View related articles 

 View Crossmark data 

Chemical characteristics of the products of the complexation reaction between copper(II) and a tetra-aza macrocycle in the presence of chloride ions

KIMBERLY M. LINCOLN[†], NETZAHUALCÓYOTL ARROYO - CURRÁS[‡],
HANNAH M. JOHNSTON[†], TRAVIS D. HAYDEN[†], BRAD S. PIERCE[§],
NATTAMAI BHUVANESH[¶] and KAYLA N. GREEN^{*†} 

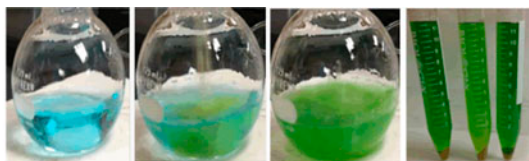
[†]Department of Chemistry, Texas Christian University, Fort Worth, TX, USA

[‡]Department of Chemistry, Center for Electrochemistry, The University of Texas at Austin, Austin, TX, USA

[§]Department of Chemistry and Biochemistry, The University of Texas at Arlington, Arlington, TX, USA

[¶]Department of Chemistry, Texas A&M University, College Station, TX, USA

(Received 10 March 2015; accepted 29 May 2015)



The reaction of copper(II) perchlorate with the hydrochloride salt of 3,6,9,15-tetra-azabicyclo[9.3.1]penta-deca-1,11,13-triene (L1) in acetonitrile forms two macrocyclic complexes that can be characterized: $[L1Cu^{II}Cl][ClO_4]$ (**1**) and $[L1Cu^{II}Cl]_2[CuCl_4]$ (**2**). The structural, electronic, and redox properties of these complexes were studied using spectroscopy (EPR and UV–visible) and electrochemistry. In addition, the solid-state structure of **1** was obtained using X-ray diffraction. The copper(II) is five-coordinate ligated by four N-atoms of the macrocycle and a chloride atom. EPR studies of **1** both in DMF and aqueous solution indicate the presence of a single copper(II) species. In contrast, EPR studies of **2** performed in frozen DMF and in the solid-state reveal the presence of two spectroscopically distinct copper(II) complexes assigned as $[L1Cu^{II}Cl]^+$ and $[Cu^{II}Cl_4]^{2-}$. Lastly, electrochemical studies demonstrate that both $[L1Cu^{II}Cl]^+$ and $[Cu^{II}Cl_4]^{2-}$ are redox active. Specifically, the $[L1Cu^{II}Cl]^+$ undergoes a quasi-reversible Cu(II)/I redox reaction in the absence of excess chloride. In the presence of chloride, however, the chemical irreversibility of this couple becomes evident at concentrations of chloride that exceed 50 mM. As a result, the presence of chloride from the chemical equilibrium of this latter species impedes the reversibility of the reduction of $[L1Cu^{II}Cl]^+$ to $[L1Cu^I Cl]^0$.

Keywords: Coordination chemistry; Copper; Electrochemistry; EPR; Macrocyclic; Pyridine; Crystallography

*Corresponding author. Email: kayla.green@tcu.edu

1. Introduction

The coordination properties of transition metal ions with tetra-aza macrocyclic ligands are an integral part of chemistry due to the inherent metal-binding nature of the tetra-amine scaffold, which mimics the naturally occurring porphyrin and corrin derivatives [1–17]. Historically, transition metal tetra-aza complexes have been utilized extensively in biomimetic inorganic chemistry as functional models for superoxide dismutase, catalase, and copper oxidase active sites [18–25]. Metal complexes derived from tetra-aza macrocyclic ligands generally present large stability constants, on the order of $\log K \geq 20.0$ in the case of copper(II) complexes [17, 18, 26–32]. In a 1969 paper by Margerum and Cabiness, the copper(II) complex derived from a tetra-aza macrocycle was determined to be 10^4 times more stable than the noncyclic tetra-amine ligand [16]. The cyclic nature of the ligand backbone leads to an increase in the kinetic and thermodynamic stability of a given metal-ion complex in solution, which is a magnitude greater than that of the *chelate effect* [16, 17, 33–35]. As a result of this enhanced stability, macrocyclic complexes show greater resistance toward metal-ion dissociation in solution when compared to an open-chain system [16, 34, 36]. This behavior, observed with N-heterocyclic ligands, is referred to as the *macrocyclic effect* [16].

Accordingly, tetra-aza macrocyclic ligands are known for the tendency to accommodate uncommon oxidation states of first-row transition metal ions in solution [23, 35, 37–50]. This is important because redox couples such as Cu(III)/(II) have rather positive reduction potentials ($E_{\text{Cu(III)/(II)}}^0 = 2.4 \text{ V}$) [51] and may be applied as redox agents in catalytic systems [52–54]. To date, several copper(II) tetra-aza complexes have been reported to undergo a reversible or quasi-reversible Cu(III/II) redox couple at solid electrodes, typically characterized by cyclic voltammetry (CV) [35–37, 42, 44, 46, 47, 50–57]. In this regard, we have noted two points. First, the work by Fabbrizzi and coworkers is unique with respect to the subsequent reports by others, because spectroscopic characterization in conjunction with electrochemical studies provided evidence for a transient macrocyclic copper(III) complex [35, 42, 46]. Second, tetra-aza macrocyclic ligands generally used for preparation of the copper(II) complexes are commonly isolated as either hydrobromide or hydrochloride salts prior to complexation with the metal-ion [6, 15, 25, 27–30, 58–62]. This latter observation is important because the presence of additional coordinating anions, such as chloride, has a profound effect on the structures of products obtained from the reaction.

In this study, we demonstrate that the reaction between copper(II) perchlorate and the hydrochloride salt of the 12-membered pyridine-based tetra-aza macrocycle 3,6,9,15-tetra-azabicyclo[9.3.1]penta-deca-1,11,13-triene (L1, shown in scheme 1) yields the expected



Scheme 1. Synthesis of L1.

[L1Cu^{II}Cl][ClO₄] complex; plus an unexpected [L1Cu^{II}Cl]₂[Cu^{II}Cl₄] species. The two products of the complexation reaction can be separated by solubility discrimination in acetonitrile solution. Structural characterization of **1** was carried out in the solid-phase by single-crystal X-ray diffraction (XRD). Solution-phase spectroscopic characterization of **1** and **2** was carried out by EPR and UV–vis spectroscopy and the redox properties investigated using CV and bulk electrolysis. Herein, we demonstrate that the presence of excess chloride hinders the chemical reversibility of the Cu(II)/(I) redox cycle associated with [L1Cu^{II}Cl]⁺ and leads to the formation of copper–chloride species. More importantly, no [L1Cu^{III}Cl]²⁺ species were observed in this work. This study represents a chemical characterization of a copper(II) tetra-aza macrocyclic complex that contains a [Cu^{II}Cl₄]²⁻ counterion and emphasizes the importance of using complementary techniques such as crystallography and spectroscopy to validate conclusions drawn from quantitative electrochemical methods.

2. Experimental studies

2.1. Materials and measurements

Caution! Perchlorate salts are explosive and should be handled in small quantities. In particular, such compounds should never be heated as solids. All chemical reagents were purchased from either Sigma-Aldrich or Alfa Aesar and used without purification. The 12-membered tetra-aza macrocycle L1 was isolated as the hydrochloride (HCl) salt prior to metal-ion complexation in accord with standard practices [63–65]. The yields reported for [L1Cu^{II}Cl][ClO₄] (**1**) and [L1Cu^{II}Cl]₂[CuCl₄] (**2**) were calculated from an average of three individual trials from the reaction carried out in acetonitrile solution. Elemental analyses were performed by Canadian Microanalytical Services Ltd. Repeated attempts to obtain suitable elemental analysis for **2** proved unsuccessful. This is likely due to co-precipitation of the complex with salts and solvent and is supported by the color changes in DMF and H₂O and the observation of CH₃CN in the unit cell of **2**.

2.2. Preparation of the 12-membered tetra-aza macrocycle (L1)

2.2.1. Synthesis of py[12]aneN₄ (L1). The 12-membered pyridine-based tetra-aza ligand [3,6,9,15-tetra-azabicyclo[9.3.1]penta-deca-1(15),11,13-triene (L1)] was prepared via (1 + 1) condensation reaction between the nosyl (Ns) amine segment and 2,6-bis(chloromethyl) pyridine. This is followed by deprotection of the amines using thiophenol and potassium hydroxide according to a modified method of the published procedure shown in scheme 1 [65]. The full synthetic details and characterization can be found in the supplemental information.

2.3. Preparation of [L1Cu^{II}Cl][ClO₄] (**1**)

A 240 mg sample of copper(II) perchlorate hexahydrate (0.65 mmol) was dissolved in 30 mL of acetonitrile. The blue solution was heated to 82 °C, and 200 mg of L1·3HCl (0.71 mmol) was added in one portion. The addition of L1 resulted in an immediate change in the color of the solution from blue to a bright greenish yellow (figure S1, see online supplemental material at <http://dx.doi.org/10.1080/00958972.2015.1068935>). Upon mixing,

the solution turned dark green. This color change was quickly followed by precipitation of **2** as an orange solid. The solution was allowed to boil for approximately two minutes further, and the temperature was reduced. The flask was capped with a septum, and the reaction was allowed to stir overnight at 70 °C. The next morning, the flask was removed from the heat and cooled to room temperature. The green solution containing the orange precipitate was transferred into three 15-mL Eppendorf tubes and centrifuged for 10 min at 4000 rpm. The supernatant was decanted and filtered through a 25-mm syringe filter into a clean 100-mL round bottom flask, and the solvent was removed under reduced pressure to yield a mixture of green and orange solids. This crude green solid was subsequently redissolved in cold acetonitrile and filtered, and the solvent was removed to yield **1** as dark green oil. Ice-cold methanol (~5 mL) was slowly pipetted into the flask followed by an equivalent volume of diethyl ether. The flask was cooled on ice for 30 min and the faintly blue-colored ether/methanol solution was discarded. The resultant solid was washed with (3 × 5 mL) portions of cold diethyl ether and dried by vacuum on a Schlenk line to afford **1** as a blue solid (63 mg, 0.13 mmol, 20% yield). Crystals suitable for X-ray analysis were obtained via slow evaporation of **1** from ethanol at room temperature. Electronic absorption, $\lambda_{\text{max}}/\text{nm}$ ($\epsilon/\text{M}^{-1} \text{cm}^{-1}$): in DMF, 794 (184) nm; MeOH, 771 (168) nm; water, 698 (122) nm. Elemental analysis for $5[\text{C}_{11}\text{H}_{18}\text{N}_4\text{CuCl}\cdot\text{ClO}_4]\cdot\text{HCl}$ found (calc.): C, 32.00 (32.07); H, 4.46 (4.45); N, 13.51 (13.60); Cl, 18.48 (18.93) %.

2.4. Isolation of $[\text{L1Cu}^{\text{II}}\text{Cl}]_2[\text{CuCl}_4]$ (**2**)

After centrifugation from the solution described above, the crude orange solid was dissolved in methanol and the resulting green solution was filtered to remove excess ligand. Next, the solvent was removed under reduced pressure to give a brownish orange solid. This resultant solid was washed with ~10 mL of cold acetonitrile, followed by ~50 mL of diethyl ether. The colorless ether/acetonitrile mixture was decanted and the dark orange solid was dried under vacuum on a Schlenk line to give **2** as a fine orange powder (150 mg, 0.26 mmol, 41% yield). Electronic absorption, $\lambda_{\text{max}}/\text{nm}$ ($\epsilon/\text{M}^{-1} \text{cm}^{-1}$): in DMF, 836 (126), 439 (600) nm; MeOH, 782 (126) nm; water, 706 (94) nm. Green powder was obtained when the synthesis was carried out in DMF with no change to the UV-vis observed. Bright green needle-like crystals of **2** were obtained from slow evaporation of an acetonitrile solution in small quantities and yielded $[\text{L1CuCl}]_2[\text{CuCl}_4]\cdot 2\text{CH}_3\text{CN}$.

2.5. Physical measurements

2.5.1. Electronic spectroscopy. The electronic spectra were collected between 200 and 1100 nm on an 8453 UV-vis spectrophotometer (Agilent) using a 3-mL quartz cuvette and with a 1.0 cm path length. The molar extinction coefficients were calculated according to the Beer-Lambert law. ^1H and ^{13}C NMR spectra were obtained on a Bruker Avance III (400 MHz) high-performance digital NMR spectrometer. The solution NMR spectroscopic analyses were carried out in CDCl_3 , D_2O , or $d\text{-DMSO}$ at 25 °C.

2.5.2. X-ray crystallographic structure determination. A Leica MZ 75 microscope was used to identify samples suitable for analysis. A Bruker Apex 2 X-ray (three-circle) diffractometer was employed for crystal screening and unit cell determination. The data collections

were obtained at 100 K. The goniometer was controlled using the APEX2 software suite, v2008-6.0 [66]. The samples were optically centered with the aid of a video camera such that no translations were observed as the crystal was rotated through all positions. The X-ray radiation employed was generated from a Mo sealed X-ray tube ($K_{\alpha} = 0.70173 \text{ \AA}$ with a potential of 40 kV and a current of 40 mA) fitted with a graphite monochromator in the parallel mode (175 mm collimator with 0.5 mm pinholes).

2.5.2.1. $[LiCu^{II}Cl][ClO_4]$. A translucent intense blue-colored block ($0.347 \times 0.360 \times 0.4877 \text{ mm}^3$) was mounted on a 0.5 mm cryoloop and used for X-ray crystallographic analysis. The crystal-to-detector distance was set to 60 mm and the exposure time was 10 s per degree for all data sets at a scan width of 0.5° . A total of 1608 frames were collected, and the data collection was 94.6% complete. The frames were integrated with the Bruker SAINT Software package [66] using a narrow frame algorithm. The integration of the data using a monoclinic unit cell yielded a total of 74,290 reflections to a maximum θ angle of 35.17° (0.62 \AA resolution) of which 12,591 were independent, with the $R_{\text{int}} = 2.29\%$. Data were corrected for absorption effects using the multi-scan method (SADABS) [67]. Structural refinements were performed with XShell (v 6.3.1) by the full-matrix least-squares method [68]. All hydrogen and nonhydrogen atoms were refined using anisotropic thermal parameters. The thermal ellipsoid molecular plots (50%) were produced using Olex 2 [69] (table 1).

2.5.2.2. $[LiCu^{II}Cl]_2[CuCl_4]$ (2). A bright green needle-like crystal ($0.035 \times 0.074 \times 0.289 \text{ mm}^3$) was mounted on a 0.5 mm cryoloop and used for X-ray crystallographic analysis. The crystal-to-detector distance was set to 50 mm, and the exposure time was 10 s per degree for all data sets at a scan width of 0.5° . A total of 1472 frames were collected. Unfortunately, the quality of the data was poor; no reflections were observed above 40° 2-theta; consequently, the reliability factors were high. Severe constraints were used to keep the bond distances, angles, and thermal ellipsoids meaningful. For analysis, sixty data frames were taken at widths of 0.5° . These reflections were used in the auto-indexing procedure to determine the unit cell using CELL_NOW [70], which suggested the presence of at

Table 1. Crystal data, intensity collections, and structure refinement parameters for $[LiCu^{II}Cl][ClO_4]$ (1).

Chemical formula	$Cu_2C_{22}H_{36}N_8Cl_2(ClO_4)_2$
MW	809.47
T (K)	100
Crystal system, space group	Monoclinic, $P2_1/c$
a, b, c (\AA)	17.788(3), 7.8071(15), 23.181(4)
α, β, γ ($^\circ$)	90, 107.523(3), 90
V (\AA^3)	3069.8(10)
Z	4
D_{calc} (g/cm^{-3})	1.751
$T_{\text{min}}, T_{\text{max}}$	0.481, 0.575
No. of measured, independent, and observed [$I > 2\sigma(I)$] reflections	74,290, 12,951, 11,864
R_{int}	0.023
Completeness to θ (%)	94.6
GOF	1.047
$R[F^2 > 2\sigma(F^2)], wR(F^2), S$	0.023, 0.062, 1.05
$\Delta\rho_{\text{max}}, \Delta\rho_{\text{min}}$ ($e \text{ \AA}^{-3}$)	0.606, -0.397

least two twin components. A suitable cell was found and refined by nonlinear least squares and Bravais lattice procedures. The absence of additional symmetry and voids were confirmed using PLATON (ADDSYM) [71]. The structure was refined (weighted least squares refinement on F^2) to convergence [69, 72]. After careful examination of the unit cell, a standard data collection procedure (four sets) was initiated using omega scans. Integrated intensity information for each reflection was obtained by reduction of the data frames with APEX2 [66]. The data were merged and scaled to produce a suitable data set. The absorption correction program TWINAB73 was employed to correct the data for absorption effects and to generate twin4.hkl and twin5.hkl. Twin4.hkl was used for structure solution as well as the final least squares refinement, as twin5.hkl did not yield better refinement. Systematic reflection conditions and statistical tests of the data suggested the space group $P2_1/n$. A solution was obtained readily using XT/XS in APEX2 [66, 72]. Two molecules of acetonitrile along with the counter anion CuCl_4^{2-} were found. Hydrogen atoms were placed in idealized positions and were set riding on the respective parent atoms. All nonhydrogen atoms were refined with anisotropic thermal parameters. One chloride showed significantly elongated thermal ellipsoid indicating disorder, which was modeled between two positions. Olex2 was employed for the final data presentation with ball-and-stick structure plots [69].

2.5.3. EPR spectroscopy. X-band (9 GHz) EPR spectra were recorded on a Bruker EMX Plus spectrometer equipped with a bimodal resonator (Bruker model 4116DM). Low-temperature measurements were made using an Oxford ESR900 cryostat and an Oxford ITC 503 temperature controller. A modulation frequency of 100 kHz was used for all EPR spectra. All experimental data used for spin quantitation were collected under nonsaturation conditions. EPR spectra were simulated and quantified using SpinCount (ver. 5.4), created by Professor M.P. Hendrich at Carnegie Mellon University [74]. The simulations were generated with consideration of all intensity factors, both theoretical and experimental, to allow concentration determination of species. The only unknown factor relating the spin concentration to signal intensity was an instrumental factor that depended on the microwave detection system. However, this was determined by the spin standard, $[\text{Cu}^{\text{II}}\text{EDTA}]^{2-}$, prepared from a copper atomic absorption standard solution purchased from Sigma-Aldrich. Component simulations of Cu(II) EPR spectra utilized for determination of g - and A -values were performed as described previously [75].

2.5.4. Electrochemistry. CV and bulk electrolysis were carried out with either an EC Epsilon potentiostat (C-3 cell stand) purchased from BASi Analytical Instruments (West Lafayette, IN) or a CH660D potentiostat from CH Instruments (Austin, TX). A glassy carbon (GC) electrode, 3 mm diameter, was also purchased from BASi (MF-2012). The electrodes were polished on a white nylon pad (BASi MF-2058) with diamond polishes of different sizes (15, 3, and 1 μm) to ensure a mirror-like finish (BASi PK-4 polishing kit MF-2060). The surface of the GC electrode was polished with the three diamond polishes each time between measurements. A three-electrode cell configuration was used with GC as the working electrode, a Ag wire (0.5 mm dia.) quasi-reference electrode housed in a glass tube (7.5 cm \times 5.7 mm) with a Porous CoralPorTM Tip, and a Pt wire (7.5 cm) as the counter electrode (BASi MW-1032). All potentials in this work are reported vs Fc/Fc^+ . The uncompensated resistance, R_u , in the electrochemical cell was not corrected in this work. For bulk electrolysis, a two-compartment cell with porous glass separators was used. The

cell was designed to hold a maximum volume of 1 mL in each compartment. Reticulated vitreous carbon from Goodfellow (Coraopolis, PA) was used in the electrolysis experiments. High mass transfer rates were achieved by mechanical stirring during electrolysis. All solutions were bubbled with argon gas for 15 min prior to experimentation and were kept under a humidified argon blanket.

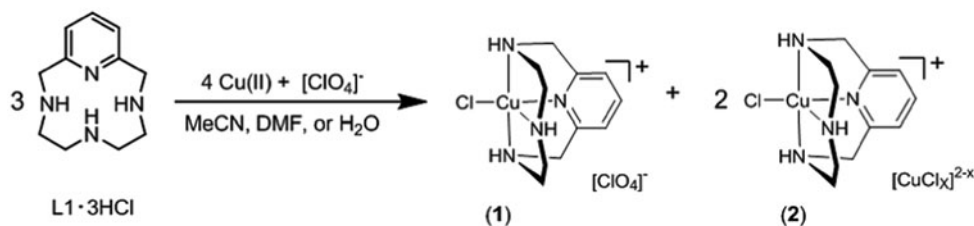
3. Results and discussion

3.1. Complexation of L1 with Cu(II) in the presence of chloride ions

Complexation between copper(II) perchlorate hexahydrate and the acid salt of L1 in nonaqueous solution gave two complexes, $[L1Cu^{II}Cl][ClO_4]$ (**1**) and $[L1Cu^{II}Cl]_2[Cu^{II}Cl_4]$ (**2**), shown in scheme 2. The addition of the hydrochloride salt of L1 to a boiling solution of copper(II) perchlorate in acetonitrile resulted in a rapid change from bright blue to green. This color change was followed by precipitation of the copper–chloride containing **2** as an orange solid. The perchlorate **1** was isolated as a light blue solid from a dark green acetonitrile solution (figure S2). The rate of formation for **2** showed dependence upon a variety of experimental factors. For example, reduction in the reaction time, temperature, or volume of acetonitrile led to a decrease in the amount of **2** formed. As a result of this sensitivity, the percent yields obtained for the two complexes varied upon subtle modification of reaction conditions. A mixture of the two products was also obtained when the complexation reaction was carried out in DMF or aqueous solution; however, **2** is soluble in these solvents. As a result, two different colored complexes were visually observed only after the removal of the solvent by rotary evaporation. Additionally, **1** and **2** were repeatedly isolated as blue and green solids, respectively, when the reactions were done in aqueous solution (figure S2). Compound **2**, obtained from aqueous solution, was partially soluble in acetonitrile. This characteristic allowed for isolation of crystalline material suitable for XRD analysis. For the studies described herein, crystalline materials isolated from the reactions in CH_3CN were used for the spectroscopic characterization described below.

3.2. Structural properties

Single-crystal X-ray crystallography was utilized to characterize the difference in structural properties between **1** and **2**. Dark blue crystals of **1** suitable for X-ray analysis were obtained from slow evaporation of ethanol at room temperature. The asymmetric unit of **1** contained



Scheme 2. Synthesis of **1** and **2**.

two independent $[\text{L1Cu}^{\text{II}}\text{Cl}][\text{ClO}_4]$ species. The molecular dimensions listed in table 2 reveal that the coordination spheres of the $[\text{L1Cu}^{\text{II}}\text{Cl}]^+$ cations have slightly different geometries [61, 76]. As shown in figure 1, the cationic $[\text{L1Cu}^{\text{II}}\text{Cl}]^+$ are five-coordinate and ligated by the four N-donors of the ligand plus a single chloride ion in a *cis*-folded fashion [1]. The four nitrogens of L1 and chloride create a distorted square pyramidal geometry ($\tau = 16\%$) around copper(II) [76]. The basal plane is defined by $[\text{N}(1), \text{N}(3), \text{N}(4), \text{and Cl}(1)]$ to give $\text{N}(1)\text{--Cu}(1)\text{--N}(3)$ and $\text{N}(4)\text{--Cu}(1)\text{--Cl}(1)$ bond angles of $153.8(3)^\circ$ and $125.6(3)$, respectively, and the axial position is occupied by $\text{N}(2)$ atom opposite to the pyridine. The $\text{N}(4)\text{--Cu}(2)\text{--N}(7)$ and $\text{N}(8)\text{--Cu}(2)\text{--Cl}(2)$ bond angles are $158.7(3)^\circ$ and $148.6(3)^\circ$ for the second $[\text{L1Cu}^{\text{II}}\text{Cl}]^+$ cation, respectively, deviating the complex toward trigonal bipyramidal ($\tau = 47\%$) [76]. This result was expected given that 12-membered ligands are not large enough to incorporate 3-D transition metal ions in a coplanar manner with respect to the N_4 plane, and agrees with reports contained in the literature for structurally similar complexes [6, 12, 28, 32, 61, 64]. The subtle geometric differences observed arise from the nonequivalence of the $\text{Cu}\text{--N}(2)$ and $\text{Cu}\text{--N}(6)$ bond lengths at $2.070(9)$ and $2.151(9)$ Å, respectively, as stronger interactions in the axial bonding interaction favor distortions toward trigonal bipyramidal [64].

Table 2. Selected metric parameters for the two independent cations of $[\text{L1Cu}^{\text{II}}\text{Cl}][\text{ClO}_4]$ (1).

Selected bond lengths (Å)			
$\text{Cu}(1)\text{--N}(1)$	2.068(9)	$\text{Cu}(2)\text{--N}(5)$	2.059(9)
$\text{Cu}(1)\text{--N}(2)$	2.151(9)	$\text{Cu}(2)\text{--N}(6)$	2.070(9)
$\text{Cu}(1)\text{--N}(3)$	2.079(9)	$\text{Cu}(2)\text{--N}(7)$	2.041(9)
$\text{Cu}(1)\text{--N}(4)$	1.956(8)	$\text{Cu}(2)\text{--N}(8)$	1.971(9)
$\text{Cu}(1)\text{--Cl}(1)$	2.247(4)	$\text{Cu}(2)\text{--Cl}(2)$	2.296(4)
Selected bond angles ($^\circ$)			
$\text{N}(1)\text{--Cu}(1)\text{--N}(3)$	158.7(3)	$\text{N}(5)\text{--Cu}(2)\text{--N}(7)$	153.8(3)
$\text{N}(4)\text{--Cu}(1)\text{--Cl}(1)$	148.6(3)	$\text{N}(8)\text{--Cu}(2)\text{--Cl}(2)$	125.6(3)
τ	0.168		0.470

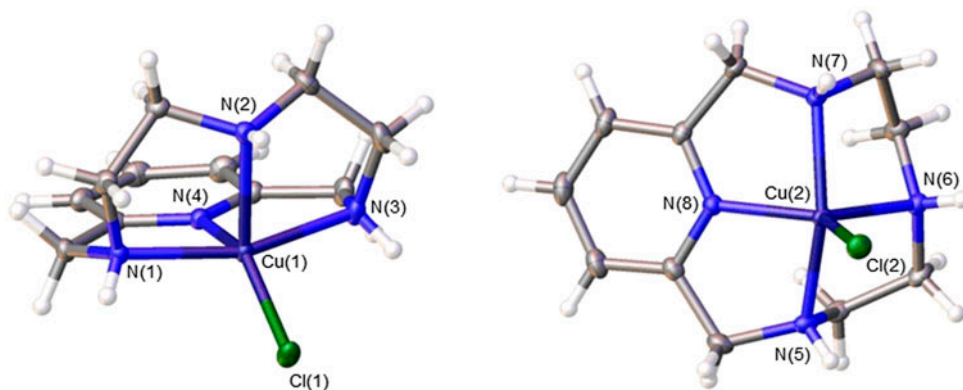


Figure 1. An ORTEP view (50% probability) of the molecular structure of $[\text{L1Cu}^{\text{II}}\text{Cl}][\text{ClO}_4]$, showing the two independent cationic species with $\tau = 0.168$ (left) and $\tau = 0.470$ (right) with the labeling scheme adopted. The two perchlorate counterions were omitted for clarity.

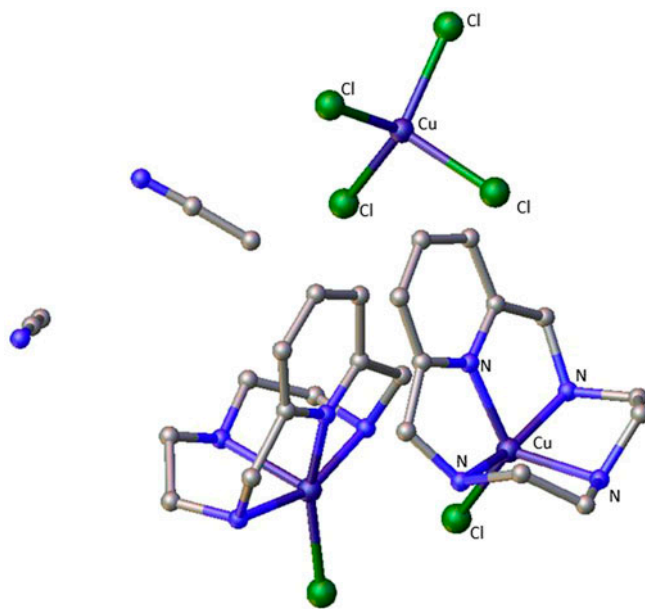


Figure 2. Ball-and-stick depiction of the crystallographically characterized complex $[L1Cu^{II}Cl]_2[Cl^{II}Cl_4]$ with the labeling scheme adopted. Hydrogens were omitted for clarity.

In contrast to **1**, bright green needle-like crystals of **2** were obtained from slow evaporation of an acetonitrile solution (figure S2) [77]. Despite twinning observed in several crystals that resulted in unpublished data, the resulting structural analysis definitively confirmed connectivity of the system and the presence of $[Cu^{II}Cl_4]^{2-}$ as a counterion for $[L1Cu^{II}Cl]^+$ (figure 2). The asymmetric unit contained four $[L1Cu^{II}Cl]^+$ cations and two $[Cu^{II}Cl_4]^{2-}$ anions with copper in the +2 oxidation state in both species. Additionally, there are a small number of reports on copper(II) tetra-aza complexes that contain $[Cu^{II}Cl_4]^{2-}$ as an anion for the cationic $[Cu^{II}N_4]^{2+}$ macrocyclic complex [62, 78–83]. In a majority of these reports, the structural and electronic properties of these complexes were characterized by XRD, UV–vis, and IR spectroscopy but the redox behaviors were largely uninvestigated.

3.3. UV–vis and EPR spectroscopy

The absorption spectra of the two complexes were measured in DMF, methanol, and aqueous solution. The energy of these transitions is similar to those for other 12-membered copper(II) tetra-aza complexes where the geometry about the metal-ion deviates between square pyramidal and trigonal bipyramidal [15, 29, 64]. The spectra of **1** and **2** shown in figure 3 reveal the coordination sphere about the copper(II) ion is dependent upon the type of solvent. For example, in DMF, **1** is light blue and contains a single d–d transition at 792 nm. In sharp contrast, **2** is bright green and contains an intense LMCT band in the visible region at 439 nm and a weaker d–d band in the near IR at 836 nm. The band observed at 439 nm is electronically equivalent to the chromophore reported for a tetrahedral $[Cu^{II}Cl_3(DMF)]^-$ species by Elleb [83] and coworkers at 440 nm. In oxygen-based solvents,

Table 3. Molar extinction coefficients calculated for **1** and **2** in DMF, MeOH, and aqueous solution.

Solvent	1	2
DMF	792 (184)	439 (600)
		836 (126)
MeOH	771 (168)	782 (126)
H ₂ O	698 (122)	706 (94)

however, **2** is light blue and the LMCT band at 439 nm is no longer observed. This result is consistent with dissociation of $[\text{Cu}^{\text{II}}\text{Cl}_3(\text{DMF})]^-$ into constituent cations and anions. In methanol and water, **1** and **2** are blue, and the d–d transitions shift to higher energy with increasing donor capability of the solvent (table 3). Overall, the magnitude of these spectral shifts indicates that each solvent evaluated coordinates in both copper(II) species.

Further characterizations of **1** and **2** were performed using X-band EPR spectroscopy. First, samples of solid materials were prepared in order to evaluate the impact of solvent on the observed signals. As illustrated in figure 4, the 10 K X-band EPR spectra collected for each $S = 1/2$ Cu-complex (**1** and **2**) are spectroscopically distinct. In the powder samples (panel A), the typical hyperfine splitting from Cu ($I = 3/2$) nuclei is unresolved due to spin–spin dipolar broadening. However, the g -values for each complex can readily be observed. Quantitative simulations for each spectrum (*dashed lines*) are overlaid on the data (*solid lines*) for comparison. The powder spectra observed in samples prepared from **2** are well fit assuming two nonequivalent copper(II)-species, which are designated as I and II in figure 4 and table 4. The component simulation of this spectrum indicates a molar contribution of 1.0–1.7 for species I and II, respectively. The copper(II) species designated (I) exhibits near axial symmetry with observable g -values of 2.34 (g_{\parallel}) and 2.06 (g_{\perp}), while species (II) appears to have a more rhombic distribution in g -values [84]. The line shape and magnitude of the g_{\parallel} -value (2.34) are nearly identical to powder spectra obtained for a variety of $[\text{CuCl}_4]^{2-}$ complexes. Powder samples prepared from **1** exhibit only a single copper(II) species with observable g -values of 2.03, 2.11, and 2.22. These values are quite similar to those observed for species (II). This finding suggests that **2** contains approximately 2 : 1 stoichiometric mixture of $[\text{L1Cu}^{\text{II}}\text{Cl}]^+$ plus another species with g -values equivalent to $[\text{Cu}^{\text{II}}\text{Cl}_4]$ [2–69, 71–84].

Solution samples of **1** and **2** were prepared in DMF and water to explore the role of solvent in complex speciation. As indicated by the UV–vis spectrum in figure 3, **2** exhibits a pronounced LMCT band at 439 nm in DMF. Figure 4(B) shows the 10 K EPR spectrum for **2** prepared in DMF (*top*). As with powder samples, the EPR spectra observed for **2** in DMF is comprised of two distinct copper(II)-species (I' and II'). Spin quantitation of these

Table 4. Simulation parameters utilized for powder and solution copper(II)-species ($S = 1/2$; $I = 3/2$).

Simulations	g -values	g -strain (σ_B)	A -values (MHz)	σ_B (mT)	Solvent
(1)	2.04, 2.10, 2.22	0.04, 0.07, 0.02	–, 100, 450	5	H ₂ O/glycerol
(2) I'	2.02, 2.07, 2.32	0.03, 0.01, 0.03	60, 60, 350	5	DMF
(2) II'	2.05, 2.07, 2.22	0.08, 0.02, 0.01	–, 70, 470	5	DMF
(1)	2.03, 2.12, 2.22	0.02, 0.02, 0.04	–	1.8	Solid
(2) I	2.05, 2.07, 2.34	0.01, 0.03, 0.03	–	1.4	Solid
(2) II	2.04, 2.16, 2.22	0.05, 0.08, 0.09	–	1.0	Solid

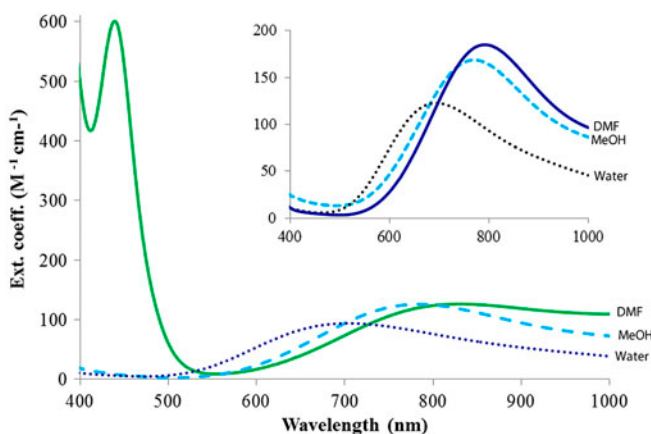


Figure 3. Electronic absorption spectra of **2** in DMF (solid line), MeOH (dashed line), and water (dotted line) at pH 5.0, showing the solvent-dependent nature of the copper(II) complexes. The inset above shows the spectra obtained for **1** in the same solvents.

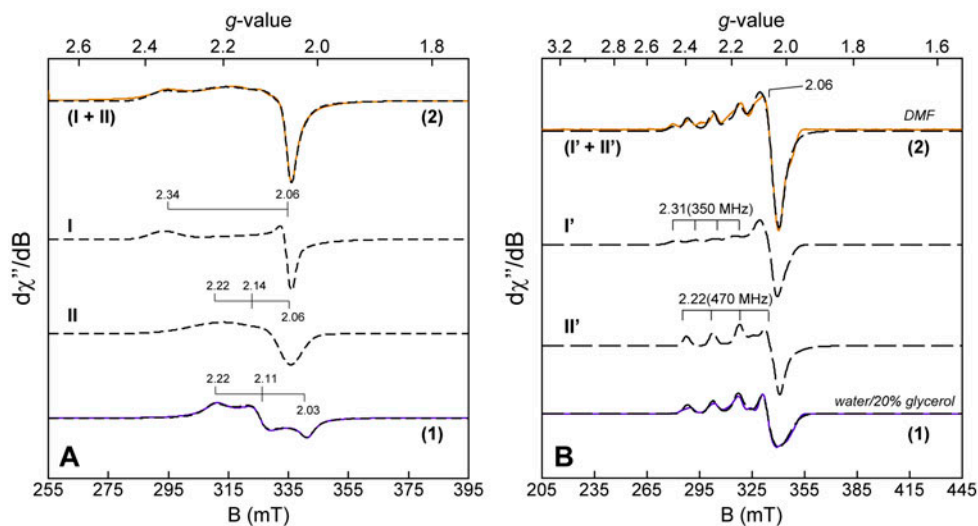


Figure 4. 10 K EPR spectrum of powder (A) and solution samples (B) of **1** and **2**. Instrumental parameters: (A) temperature, 10 K; microwave frequency, 9.65 GHz; microwave power, 2 μ W (A) and 6 μ W; (B) modulation amplitude, 0.92 mT. Simulation parameters utilized for **1** and **2** species I/I' and II/II' are provided in table 4.

two species accounts for 93% of the total Cu in the sample (2.8 mM). For clarity, the copper(II)-species observed in solution are designated by I' and II' to differentiate these spectra from I and II observed in powder samples. Species I' exhibits near axial symmetry $g_{x,y,z} = 2.02, 2.07,$ and 2.32 with hyperfine splitting aligned along the g_1 -axis ($A_1 \sim 350$ MHz). The magnitude of the g_1 -value (2.32) and near axial symmetry is consistent with species I observed in powder spectra of **2**. The copper(II)-species II' also exhibits a nearly axial spectrum $g_{x,y,z} = 2.05, 2.07, 2.22$ but with a significantly larger A_1 -value

(470 MHz). The simulation of species II also includes unresolved hyperfine along the g_y -axis to model the observed line width ($A_y \sim 70$ MHz). However, this could also be fit assuming increased g -strain along this axis or contributions from both g -strain and unresolved hyperfine. The g -spread (Δg) is quite similar for II and II'; however, the observed g -anisotropy appears more pronounced for solid samples (II). This finding may indicate some geometric perturbations induced by solvent interactions.

For comparison, aqueous samples of **1** were prepared using 20% glycerol as a glassing agent to prevent inter-molecular aggregation. As seen in figure 3, UV-visible spectroscopy indicates that in aqueous solution, the LMCT band 439 nm is absent. In these samples, the 10 K EPR spectra are readily simulated using a single copper(II) species with $g_{x,y,z} = 2.06, 2.10, \text{ and } 2.22$; $A_1 = 450$ MHz. A quantitative simulation (*dashed line*) is overlaid on the spectra for comparison. Additional validation of the spectroscopic parameters determined for aqueous samples of **1** can be taken from the near stoichiometric (94%) quantitation of copper(II) predicted by spectroscopic simulation. The microwave power required for half-saturation ($P_{1/2}$) of the signals was measured at $120 \pm 10 \mu\text{W}$ at 10 K. As with II', the line width along the g_y -axis is approximated by unresolved hyperfine ($A_y \sim 100$ MHz). Remarkably, the observed g -values for aqueous samples of (**1**) are closely matched to what is observed in powder samples prepared from **1**. Based on comparable g_1 and A_1 -values, species II and II' observed in powder and solution samples of **2** are likely attributed to the single species observed in samples of **1**. By extension, species I and I' observed in samples prepared from **2** are assigned to formation of a $[\text{CuCl}_4]^{2-}$ counterion. This conclusion is consistent with the results obtained by UV-visible spectroscopy and supports the assignment of the optical transition at 439 nm to a copper-to-chloride LMCT band [83].

3.4. Redox properties: electrochemical studies

The electrochemistry of **1** and **2** was studied by CV and bulk electrolysis in order to investigate the redox behavior of the complexes in solution. As illustrated in figure 5, the electrochemical behaviors of **1** and **2** are independent from one another. In the studies presented below, the solids obtained from the reaction in aqueous solution (*green solid*) and in acetonitrile solution (*blue and orange solids*) were analyzed individually. The green solid isolated from the reaction in aqueous solution containing a mixture of both complexes was initially evaluated. In this experiment, a 6.7 mg sample of the green solid was dissolved in DMF and analyzed with a GC working electrode, shown in figure 5(A). The open circuit potential (OCP) of the system was 0.95 V. When the electrode potential was scanned from the OCP to -0.70 V and then reversed, the current-potential curve showed two redox waves at 0.60 and -0.25 V. These redox waves correspond to the reduction in each of the two different copper(II) species present in solution $[\text{CuCl}_x]^{2-x}$ and $[\text{L1Cu}^{\text{II}}\text{Cl}]^+$ [figure 5(A)]. This finding is in contrast to our most recent report, where the more positive and quasi-reversible redox wave was postulated to be a Cu(III)/(II) redox couple [64]. To further confirm these assignments, the two complexes isolated from acetonitrile were independently studied by CV and bulk electrolysis.

Figure 5(B) shows the CVs of **1** and **2** recorded in DMF. The black trace is a CV recorded with a GC working electrode in the absence of redox active species, and the red trace is the CV of **1** recorded in DMF. The red trace shows only one redox wave at $E_1 = -0.25$ V. This redox process corresponds to the quasi-reversible reduction ($\Delta E_p = 85$ mV, R_u not corrected) of $[\text{L1Cu}^{\text{II}}\text{Cl}]^+$ to $[\text{L1Cu}^{\text{I}}\text{Cl}]^0$ in the absence of the $[\text{Cu}^{\text{II}}\text{Cl}_4]^{2-}$ counterion. The reaction is diffusion controlled [85] as determined by plots of

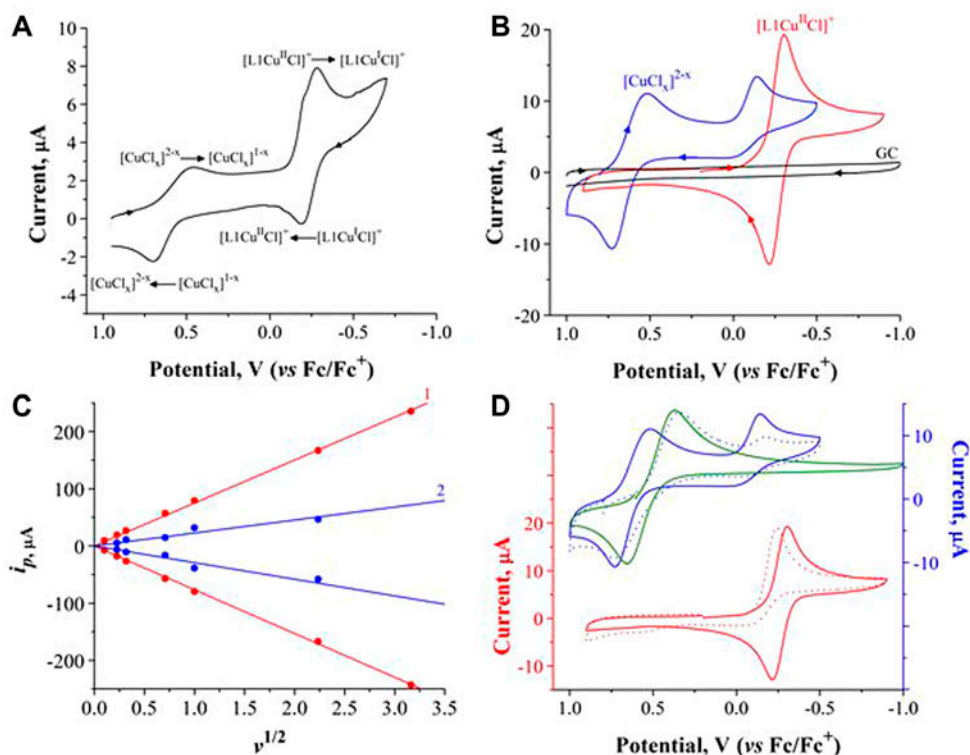
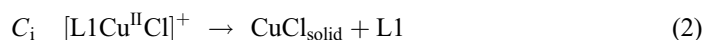
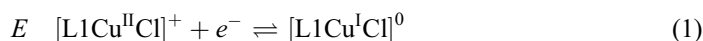


Figure 5. (A) CV recorded with a glassy carbon (GC) electrode (dia. = 2 mm) in DMF solution containing 6.7 mg of the products of the synthesis reaction before purification +0.1 M TBAP. The arrows in all voltammograms indicate the direction of the potential scans, (B) CVs of GC electrode in 0.1 M TBAP in DMF (black), 2.3 mM (1) + 0.1 M TBAP in DMF (red), and 2.0 mM (2) + 0.1 M TBAP in DMF (blue), (C) Plots of anodic and cathodic peak currents, i_p , vs. $\nu^{1/2}$. $\nu = 0.05, 0.1, 0.5, 1.0, 5.0,$ and 10.0 V s^{-1} , and (D) (Top) CVs of 2.0 mM (2) + 0.1 M TBAP in DMF in the absence (solid blue) and presence (dashed blue) of 100 mM Cl^- , and CV of 2 mM Cu(II) + 0.1 M TBAP + 100 mM Cl^- in DMF (green). The current axis is shown on the right side of the plot. (Bottom) CVs of 2.3 mM (1) + 0.1 M TBAP in DMF in the absence (solid red) and presence (dashed red) of $[\text{LiCl}] = 100 \text{ mM}$. The current axis is shown on the left side of the plot (see <http://dx.doi.org/10.1080/00958972.2015.1068935> for color version).

cathodic and anodic peak currents, i_p , versus $\nu^{1/2}$ ($\nu = \text{scan rate}$), shown as red dots in figure 5(C). Bulk electrolysis of $[\text{L1Cu}^{\text{II}}\text{Cl}]^+$ to $[\text{L1Cu}^{\text{I}}\text{Cl}]^0$ gave $n = 1$ and revealed an EC_i reaction (data provided as supporting information):



The EC_i reaction is supported by appearance of a green precipitate of copper–chloride on the surface of the electrode during electrolysis of **1** (figure S3). Importantly, the appearance of copper–chloride during electrolysis implied that $\log \beta_{\text{copper(II)}} \gg \log \beta_{\text{copper(I)}}$ of the heterocyclic ligand L1 [8, 37, 86]. This behavior was further studied by carrying out CV in solutions containing chloride ions, shown in figure 5(D). When a copper-to-chloride ratio of 1 : 50 was used, the reduction current of $[\text{L1Cu}^{\text{II}}\text{Cl}]^+$ to $[\text{L1Cu}^{\text{I}}\text{Cl}]^0$ remained unchanged,

but the reverse anodic reaction disappeared completely (red dotted trace in figure 5(D)). Less dramatic effects in the magnitude of the anodic current were observed at lower concentrations of chloride.

The blue trace in figure 5(B) is the CV of **2** in DMF solution. This solution contained the same species discussed in figure 4(B). When the electrode potential was scanned from the OCP of 0.75 to -0.50 V and reversed back, the current–potential curve showed two redox waves at 0.60 and -0.25 V. The wave at $E_2 = 0.60$ V corresponds to quasi-reversible reduction ($\Delta E_p = 210$ mV) of $[\text{CuCl}_x]^{2-x}$ to $[\text{CuCl}_x]^{1-x}$. This reaction is diffusion controlled as shown in figure 5(C). Bulk electrolysis of $[\text{CuCl}_x]^{2-x}$ to $[\text{CuCl}_x]^{1-x}$ gave $n = 1$ and the electrolysis were reversible, giving the same number of Coulombs in forward and reverse reactions (figure S4). Moreover, the second reduction wave corresponds to the reduction of $[\text{LiCu}^{\text{II}}\text{Cl}]^+$ to $[\text{LiCu}^{\text{I}}\text{Cl}]^0$. Importantly, since this solution contained chloride, no reverse wave was observed. In this case, the equilibria between Cu(II), Cu(I), and chloride control the electrochemical behavior of the complex system. Thus, in order to understand how the presence of chloride ions affected the reversibility of the Cu(II)/Cu(I) redox cycle of the macrocyclic complex, excess chloride was intentionally added.

As shown in figure 5(D), the addition of lithium chloride altered the shape of the resulting voltammograms. When a copper(II)-to-chloride ratio of 1 : 50 was used, for example, the current corresponding to the reduction of $[\text{LiCu}^{\text{II}}\text{Cl}]^+$ to $[\text{LiCu}^{\text{I}}\text{Cl}]^0$ decreased by half and the wave corresponding to the $[\text{CuCl}_x]^{2-x}/[\text{CuCl}_x]^{1-x}$ redox reaction shifted 80 mV to less positive potentials (blue dotted trace in figure 5(D)). These observations were expected since the addition of chloride to a solution containing copper(II) shifts the chemical equilibrium to favor the formation of new CuCl_x^{2-x} species [83]. Finally, a control experiment was carried out to support the claim that the redox wave at 0.60 V is related to a $[\text{CuCl}_x]^{2-x}/[\text{CuCl}_x]^{1-x}$ couple, as opposed to the Cu(III)/Cu(II) couple [64]. In this experiment, CV studies were carried out in a solution of 2 mM Cu(II) + 100 mM LiCl in the absence of the ligand. This CV is shown by the green trace in figure 5(D). As expected, a good correlation in the shape and potential was observed when overlaying the CVs recorded with $[\text{Cl}^-] = 100$ mM in the absence and presence of L1, shown in figure 5(D). The conclusions obtained from the electrochemical analyses are in agreement with the structural and spectroscopic data discussed previously.

4. Conclusion

Copper(II) complexation reactions with tetra-aza macrocyclic ligands, when isolated as hydrochloride salts, can lead to unexpected inorganic copper–chloride species plus the target macrocyclic complex. The $[\text{Cu}^{\text{II}}\text{Cl}_4]^{2-}$ species was formed in both aqueous and nonaqueous solution concomitant to complexation of copper(II) with the N-heterocyclic ligand, but formation of these pure inorganic species was not spectroscopically detectable due to dissociation in aqueous or oxygen-containing solvents. This finding has important implications when analyzing the electrochemical properties of these types of complexes, because both $[\text{Cu}^{\text{II}}\text{Cl}_4]^{2-}$ and $[\text{LiCu}^{\text{II}}\text{Cl}]^+$ species were determined to be electrochemically active. Given certain underlying assumptions regarding the redox nature of copper(II) tetra-aza macrocyclic complexes, one may misinterpret the redox activity of the metal-halide species for that of the macrocyclic complex. Therefore, when asserting that copper(II) tetra-aza complexes can undergo a Cu(III)/(II) redox cycle it is imperative the electrochemical findings are supported via structural and spectroscopic characterization of the proposed copper(III) species [87].

Supporting information

Synthetic details for L1 and bulk electrolysis experimental data along with crystallographic information for complex (1) (CCDC # 1018080) in both CIF and table format are accessible. This material is available free of charge via the Internet at <http://pubs.acs.org>.

Acknowledgements

The authors are grateful for generous financial support from NSF (CHE) 1213655 to B.S.P., TCU Andrews Institute of Mathematics & Science Education (to KG), TCU Research and Creativity Activity Grant (to KG), INFOR Moncrief Foundation Support (to KG), and the Robert A. Welch Foundation (to KG, P-1760). The authors are grateful for the help from collaborates regarding the electrochemical, EPR, and X-ray crystallography studies. We thank the research group of Dr Allen Bard at Center for Electrochemistry, University of Texas at Austin and Bruce Noll, Bruker AXS.

Disclosure statement

The authors declare no competing financial interest.

ORCID

Kayla N. Green  <http://orcid.org/0000-0001-8816-7646>

References

- [1] D.H. Busch. *Acc. Chem. Res.*, **11**, 392 (1978).
- [2] N. Takvoryan, K. Farmery, V. Katovic, F.V. Lovecchio, E.S. Gore, L.B. Anderson, D.H. Busch. *J. Am. Chem. Soc.*, **96**, 731 (1974).
- [3] V. Amendola, L. Fabbrizzi, C. Mangano, H. Miller, P. Pallavicini, A. Perotti, A. Taglietti. *Angew. Chem.*, **114**, 2665 (2002).
- [4] M. Carter, M. Rodriguez, A. Bard. *J. Am. Chem. Soc.*, **111**, 8901 (1989).
- [5] M.Y. Chavan, T.J. Meade, D.H. Busch, T. Kuwana. *Inorg. Chem.*, **25**, 314 (1986).
- [6] C. Esteves, L. Lima, P. Mateus, R. Delgado, P. Brandão, V. Félix. *Dalton Trans.*, **42**, 6149 (2012).
- [7] P. Comba, M. Kubeil, J. Pietzsch, H. Rudolph, H. Stephan, K. Zarschler. *Inorg. Chem.*, **53**, 698 (2014).
- [8] K. Woodin, K. Heroux, C. Boswell, E. Wong, G. Weisman, W. Niu, S. Tomellini, C. Anderson, L. Zakharov, A. Rheingold. *Eur. J. Inorg. Chem.*, 4829 (2005).
- [9] L. Fabbrizzi, M. Licchelli, P. Pallavicini, A. Perotti, A. Taglietti, D. Sacchi. *Chem. Eur. J.*, **2**, 75 (1996).
- [10] P. Goswami, D. Das. *J. Fluoresc.*, **22**, 1081 (2012).
- [11] X. Huang, Y. Lu, Y. He, Z. Chen. *Eur. J. Org. Chem.*, 1921 (2010).
- [12] J.-H. Wen, C.-Y. Li, Z.-R. Geng, X.-Y. Ma, Z.-L. Wang. *Chem. Commun.*, **47**, 11330 (2011).
- [13] X. Wang, X. Ma, Z. Yang, Z. Zhang, J. Wen, Z. Geng, Z. Wang. *Chem. Commun.*, **49**, 11263 (2013).
- [14] S. El Ghachtouli, C. Cadiou, I. Déchamps-Olivier, F. Chuburu, M. Aplincourt, V. Patinec, M. Le Baccon, H. Handel, T. Roisnel. *New J. Chem.*, **30**, 392 (2006).
- [15] M. Styka, R. Smierciak, E. Blinn, R. DeSimone, J. Passariello. *Inorg. Chem.*, **17**, 82 (1978).
- [16] D. Cabbiness, D. Margerum. *J. Am. Chem. Soc.*, **91**, 6540 (1969).
- [17] D.K. Cabbiness, D.W. Margerum. *J. Am. Chem. Soc.*, **92**, 2151 (1970).
- [18] M. Munakata, J. Endicott. *Inorg. Chem.*, **23**, 3693 (1984).
- [19] N. Raffard, R. Carina, A.J. Simaan, J. Sainton, E. Rivière, L. Tchertanov, S. Bourcier, G. Bouchoux, M. Delroisse, F. Banse. *J. Girerd. Eur. J. Inorg. Chem.*, 2249 (2001).
- [20] L. Koziol, C. Valdez, S. Baker, E. Lau, W. Floyd, S. Wong, J. Satcher, F. Lightstone, R. Aines. *Inorg. Chem.*, **51**, 6803 (2012).

- [21] C. Bailey, R. Bereman, D. Rillema. *Inorg. Chem.*, **25**, 3149 (1986).
- [22] F. Abba, G. De Santis, L. Fabbrizzi, M. Licchelli, A. Manotti Lanfredi, P. Pallavicini, A. Poggi, F. Ugozzoli. *Inorg. Chem.*, **33**, 1366 (1994).
- [23] W. Ye, D. Ho, S. Friedle, T. Palluccio, E. Rybak-Akimova. *Inorg. Chem.*, **51**, 5006 (2012).
- [24] V. Bansal, R. Kumar, R. Prasad, S. Prasad, N. Niraj. *J. Mol. Catal. A: Chem.*, **284**, 69 (2008).
- [25] M.H. Salter, J.H. Reibenspies, S. B. Jones, R.D. Hancock. *Inorg. Chem.*, **44**, 2791 (2005).
- [26] C. Castillo, J. González-García, J. Llinares, M. Máñez, H. Jimenez, E. García-España, M. Basallote. *Dalton Trans.*, **42**, 6131 (2013).
- [27] K. Guerra, R. Delgado, V. Félix. *Dalton Trans.*, 4124 (2006).
- [28] V. Félix, M.J. Calhorda, J. Costa, R. Delgado, C. Brito, M.T. Duarte, M.G. Drew. *J. Chem. Soc., Dalton Trans.*, 4543 (1996).
- [29] J. Costa, R. Delgado. *Inorg. Chem.*, **32**, 5257 (1993).
- [30] R. Delgado, S. Quintino, M. Teixeira, A. Zhang. *J. Chem. Soc., Dalton Trans.*, 55 (1997).
- [31] A. Fernandes, M. Cabral, J. Costa, M. Castro, R. Delgado, M. Drew, V.J. Félix. *Inorg. Biochem.*, **105**, 410 (2011).
- [32] M. Inclán, M. Albelda, J. Frías, S. Blasco, B. Verdejo, C. Serena, C. Salat-Canela, M. Díaz, A. García-España, E. García-España. *J. Am. Chem. Soc.*, **134**, 9644 (2012).
- [33] L. Fabbrizzi, P. Paoletti, A.B.P. Lever. *Inorg. Chem.*, **15**, 1502 (1976).
- [34] L. Chen, C. Chung. *Inorg. Chem.*, **27**, 1880 (1988).
- [35] L. Fabbrizzi, T. Kaden, A. Perotti, B. Seghi, L. Siegfried. *Inorg. Chem.*, **25**, 321 (1986).
- [36] L.F. Lindoy. *The Chemistry of Macrocyclic Ligand Complexes*, Cambridge University Press, New York, NY (1989).
- [37] L. Fabbrizzi, A. Poggi, P. Zanello. *J. Chem. Soc., Dalton Trans.*, 2191 (1983).
- [38] L. Fabbrizzi, M. Licchelli, G. De Santis, N. Sardone, A. Velders. *Chem. Eur. J.*, **2**, 1243 (1996).
- [39] A. Buttafava, L. Fabbrizzi, A. Perotti, A. Poggi, G. Poli, B. Seghi. *Inorg. Chem.*, **25**, 1456 (1986).
- [40] A. Bencini, L. Fabbrizzi, A. Poggi. *Inorg. Chem.*, **20**, 2544 (1981).
- [41] K.E. Barefield, D.H. Busch. *J. Chem. Soc., Chem. Commun.*, 522 (1970).
- [42] L. Fabbrizzi, A. Poggi. *J. Chem. Soc., Chem. Commun.*, 646 (1980).
- [43] G. Golub, H. Cohen, D. Meyerstein. *J. Chem. Soc., Chem. Commun.*, 397 (1992).
- [44] I. Fritsky, H. Kozlowski, O. Kanderl, M. Haukka, J. Swiatek-Kozlowska, E. Gumienka-Kontecka, F. Meyer. *Chem. Commun.*, 4125 (2006).
- [45] N. Jubran, H. Cohen, Y. Koresh, D. Meyerstein. *J. Chem. Soc., Chem. Commun.*, 1683 (1984).
- [46] C.B. Castellani, L. Fabbrizzi, M. Licchelli, A. Perotti, A. Poggi. *J. Chem. Soc., Chem. Commun.*, 806 (1984).
- [47] S. Domagala, J. Malecka, A. Michalowicz, I. Mames, B. Kamiński, M. Woźny, R. Bilewics, B. Korubut-Daszkiwicz, K. Woźniak. *Eur. J. Inorg. Chem.*, 3680 (2012).
- [48] T.J. Hubin, N.W. Alcock, D.H. Busch. *Acta Crystallogr., Sect. C: Cryst. Struct. Commun.*, **56**, 37 (2000).
- [49] W.O. Koch, J.T. Kaiser, H.J. Kruger. *Chem. Commun.*, 2237 (1997).
- [50] L. Fabbrizzi. *Comments Inorg. Chem.*, **4**, 33 (1985).
- [51] W.M. Haynes (Ed.). *CRC Handbook of Chemistry and Physics*, 95th Edn, pp. 5–81, CRC Press, Boca Raton (2014).
- [52] R. Zifra, X. Ribas, A. Llobet, A. Poater, M. Duran, M. Solà, T. Stack, J. Benet-Buchholz, B. Donnadiu, J. Mahia, T. Parella. *Chem. Eur. J.*, **11**, 5146 (2005).
- [53] F. Monnier, M. Taillefer. *Angew. Chem. Int. Ed.*, **48**, 6954 (2009).
- [54] A. Casitas, X. Ribas. *Chem. Sci.*, **4**, 2301 (2013).
- [55] T. Hubin, N. Alcock, M. Morton, D. Busch. *Inorg. Chim. Acta*, **348**, 33 (2003).
- [56] K.Y. Choi. *J. Chem. Crystallogr.*, **34**, 603 (2004).
- [57] K. Jeyasubramanian, S. Samath, S. Thambidurai, R. Murugesan, S. Ramalingam. *Transition Met. Chem.*, **76** (1995).
- [58] P. Zanello, R. Seeber, A. Cinquantini, G.-A. Mazzocchin, L. Fabbrizzi. *J. Chem. Soc., Dalton Trans.*, 893 (1982).
- [59] L. Fabbrizzi, F. Forlini, A. Perotti, B. Seghi. *Inorg. Chem.*, **23**, 807 (1984).
- [60] S. Srinivasan, P. Athappan. *Transition Met. Chem.*, **26**, 588 (2001).
- [61] V. Félix, J. Costa, R. Delgado, M. Drew, M. Duarte, C. Resende. *J. Chem. Soc., Dalton Trans.*, 1462 (2001).
- [62] B.M. Yamin, W. Ismail, J.C. Daran. *Acta Crystallogr. Sect. E: Struct. Rep. Online*, **68**, 886 (2012).
- [63] K. Lincoln, T. Richardson, L. Rutter, P. Gonzalez, J. Simpkins, K. Green. *ACS Chem. Neurosci.*, **3**, 919 (2012).
- [64] K. Lincoln, M. Offutt, T. Hayden, R. Saunders, K. Green. *Inorg. Chem.*, **53**, 1406 (2014).
- [65] J.-M. Siaugue, F. Segat-Dioury, I. Sylvestre, A. Favre-Régouillon, J. Foos, C. Madic, A. Guy. *Tetrahedron*, **57**, 4713 (2001).
- [66] Bruker Advanced X-ray Solutions. *APEX2 (Version 2014.9-0)*, Bruker AXS Inc., Madison, WI (2007).
- [67] Bruker Advanced X-ray Solutions. *SADABS*, Bruker AXS Inc., Madison, WI (2001).
- [68] Bruker Advanced X-ray Solutions. *XSELL (Version 6.3.1)*, Bruker AXS Inc., Madison, WI (2004).

- [69] O.V. Dolomanov, L.J. Bourhis, R.J. Gildea, J.A.K. Howard, H. Puschmann. *J. Appl. Crystallogr.*, **42**, 339 (2009).
- [70] (a) A.L. Spek. *J. Appl. Crystallogr.*, **36**, 7 (2003); (b) A.L. Spek. *PLATON – A Multipurpose Crystallographic Tool.*, Utrecht University, Utrecht (2008).
- [71] G.M. Sheldrick. *Cell_Now Program for Obtaining Unit Cell Constants from Single Crystal Data (Version 2008/4)* University of Göttingen, Göttingen (2008).
- [72] G.M. Sheldrick. *Acta Crystallogr., Sect. A: Found. Crystallogr.*, **A64**, 112 (2008).
- [73] Bruker Advanced X-ray Solutions, G. M. Sheldrick. *TWINABS* Bruker AXS Inc., Madison, WI (2001).
- [74] A.P. Golombek, M.P. Hendrich. *J. Magn. Reson.*, **165**, 33 (2003).
- [75] D.M. Arciero, B.S. Pierce, M.P. Hendrich, A.B. Hooper. *Biochemistry*, **41**, 1703 (2002).
- [76] A.W. Addison, N.T. Rao, J. Reedijk, J. van Rijn, G.C. Verschoor. *J. Chem. Soc., Dalton Trans.*, 1349 (1984).
- [77] Unit cell: $P2_1/n$. $a = 15.875(4)$, $b = 7.541(2)$, $c = 26.207(3)$ Å, $\beta = 103.37(2)^\circ$, $V = 3052.5(12)$ Å³, $Z = 8$.
- [78] P. Comba, N.F. Curtis, G.A. Lawrance, M.A. O'Leary, B.W. Skelton, A.H. White. *J. Chem. Soc., Dalton Trans.*, 497 (1988).
- [79] I. Vasilevsky, N.R. Rose, R. Stenkamp, R.D. Willett. *Inorg. Chem.*, **30**, 4082 (1991).
- [80] Z. Wang, R. Willett, S. Molnar, K. Brewer. *Acta Crystallogr., Sect. C: Cryst. Struct. Commun.*, **52**, 581 (1996).
- [81] U. Suksangpanya, A. Blake, P. Hubberstey, C. Wilson. *Crystallogr. Eng. Commun.*, **4**, 552 (2002).
- [82] M. Studer, A. Riesen, T. Kaden. *Helv. Chim. Acta*, **72**, 1253 (1989).
- [83] M. Elleb, J. Meullemeestre, M. Schwing-Weill, F. Vierling. *Inorg. Chem.*, **19**, 2699 (1980).
- [84] A. Winter, K. Thiel, A. Zabel, T. Klamroth, A. Pöpl, A. Kelling, U. Schilde, A. Taubert, P. Strauch. *New J. Chem.*, **38**, 1019 (2013).
- [85] A.J. Bard, L.R. Faulkner. *Electrochemical Methods Fundamentals and Applications*, 2nd Edn., Wiley, Hoboken (2001).
- [86] L. Sabatini, L. Fabbrizzi. *Inorg. Chem.*, **18**, 438 (1978).
- [87] E. Rountree, B. McCarthy, T. Eisenhart, J. Dempsy. *Inorg. Chem.*, **53**, 9983 (2014).